Chalcogenide Letters Vol. 18, No. 9, September 2021, p. 513 - 523

Radiation protection assessment of gamma photons in $64TeO_2$–$10WO_3$–$10Nb_2O_5$–$15KF$–$1La_2O_3$ glasses doped with Tm_2O_3 using photon-shielding and dosimetry software

A. M. Alqahtani[a,*], M. S. Alqahtani[b,c], K. I. Hussein[b,d], A. J. Alkulib[b], F.F. Alqahtani, E. Yousef[g,h,i]

[a]*Medical and Clinical Affairs Department, King Faisal Medical City, Abha 62523, Saudi Arabia*

[b]*Department of Radiological Sciences, College of Applied Medical Sciences, King Khalid University, Abha 61421, Saudi Arabia*

[c]*BioImaging Unit, Space Research Centre, Department of Physics and Astronomy, University of Leicester, Leicester LE1 7RH, UK*

[d]*Department of Medical Physics and Instrumentation, National Cancer Institute, University of Gezira, Wad Medani 20, Sudan*

[e]*Department of Radiological Sciences, College of Applied Medical Sciences, Najran University, Najran 1988, Saudi Arabia*

[g]*Research Center for Advanced Materials Science (RCAMS), King Khalid University, Abha 61421, Saudi Arabia*

[h]*Physics Department, Faculty of Science, King Khalid University, Abha 61421, Saudi Arabia*

[i]*Physics Department, Faculty of Science, Al Azhar University, Assiut branch, Egypt*

Radiation-shielding applications are necessary to protect against deleterious effects of radiation. This study tested thulium oxide (Tm_2O_3) added to the glass-system composition $64TeO_2$–$10WO_3$–$10Nb_2O_5$–$15KF$–$1La_2O_3$. Adding Tm_2O_3 increased sample density from 5.22 to 5.40 g/cm^3 and measured at photon energy of 15 keV–15 MeV. Multiple radiation-shielding parameters were evaluated and assessed using photon-shielding and dosimetry software, including linear and mass attenuation coefficients, half-value layers, mean free paths, atomic and electronic cross sections, effective atomic numbers, effective electron density, and exposure buildup factors. Half-value layer and mean free-path values were compared with those of well-known radiation-shielding materials, ie, conventional concrete and commercial glasses. Atomic and electronic cross-section values effectively increased with the addition of thulium oxide to the glass systems. While the highest linear and attenuation coefficients were 242–281 cm^2/g at 15 keV, the denser glass recorded the highest mass attenuation coefficients value of 52.17 cm^2/g across all samples. The highest effective atomic number and effective electron density were recorded for the denser glass, because it had the highest thulium oxide fraction and was more burdened by interaction with photon energy. Half-value layers and mean free paths showed similar behavior, and high-density materials achieved low values. At high energy, exposure buildup-factor values increased, while at low energy, values decreased.

(Received June 23, 2021; Accepted September 8, 2021)

Keywords: Radiation shielding, Phy-X/SPD, Interaction of radiation with materials

1. Introduction

Ionizing radiation, such as X-rays and γ-rays, is used in medical imaging and other industries. Radiation plays an important role in enhancing diagnosis and therapy in the medical field and can also be used in antiquity research, food processing, nuclear research centers, the generation of electricity, and other industries (1–3). However, several reports have shown that

* Corresponding author: a.m.qahtani@kfmcity.med.sa

https://doi.org/10.15251/CL.2021.189.513

exposing living tissue to unsafe or unknown leaking ionizing radiation can cause serious biological damage in humans and lead to death (4–6). As a result, reducing the risk to those who work directly with ionizing radiation, such as medical staff, must be taken into account to avoid any risks. As a result, shielding has become a popular area of research, focusing on reducing serious hazards caused by radiation exposure to human beings by validating practical, scientific methods to protect living tissue (7–9). Lead (Pb) has been used widely for protection against radiation, and lead with other diverse chemical components has been assessed and evaluated against a broad spectrum of ionizing radiation energy. Its use is confined because it is extremely toxic, costly, heavy, and has a low melting point (10,11). However, glass is an alternative material, along with ceramics, concrete, alloys, and polymers, that are powerful against ionizing radiation, inexpensive, and with low toxicity compared to lead (10).

Glass has been utilized to prevent and reduce radiation effects and risks for the general public and the environment. In place of lead, an appropriate option for radiation protection could be high-density, oxide-based glass with low melting point and crystallization ability, good transparency for visible light, high thermal stability, and 100% recyclability (12–14). Such glass would be useful for different applications, eg, medical imaging, and in various compositions that have been tested in radiation-protection applications. A novel high-density oxide-based glass formation could be developed for testing against different-energy ionizing radiation. The possibility of using tellurium dioxide (TeO_2) glass as shielding for protection against a variety of ionizing-radiation energies has been shown in numerous studies (10,13,15–17), The refractive index in Tm_2O_3 glass has been noted for its high values and widely infrared transmittance, as well as appropriately high phonon energy to ~ 750 cm^{-1}(18,19). Moreover, with a low melting point, TeO_2 is stable and has good ability to form as glass because of its high refractive index and reducing the optical energy gap, as well as cleavage of nonbridging oxygen in the structure (20).

TeO_2's physical and chemical properties have been studied and compared to other oxide glass, such as phosphate and silicates, for use in different applications (21). Recently, TeO_2 in glass compositions has drawn significant interest for many different applications and technologies. Radiation protection is one of these applications, because the TeO_2-glass systems have high mass density, good durability and transparency, and the capability of blocking more photons (22–25). A glass system based on TeO_2–WO_3–Nb_2O_5–KF–La_2O_3 and doped with different amounts of Tm_2O_3 was assessed on various parameters using photon-shielding and dosimetry software (Phy-X/PSD), which can generate data with a range of energy (1 keV to 100 GeV) and some radioactive sources, such as ^{133}Ba (26). This study evaluated the behavior of these compositions by assessing their radiation-protection parameters, including linear and mass attenuation coefficients (LACs and MACs), half and tenth value layers (HVLs), mean free paths (MFPs), atomic and electronic cross sections (ACSs and ECSs), effective atomic and electron numbers (Z_{eff} and N_{eff}), and exposure buildup factors (EBFs).

Table 1. The composition, wights, density and molar volume of the glasses samples.

Glass Sample	TeO_2	WO_3	Nb_2O_5	KF	La_2O_3	Tm_2O_3	Density (g/cm^3)	V_M (cm^3. mol^{-1})
S1	64	10	10	15	1.0	-	5.22	31.39
S2	64	10	10	15	1.0	1.0	5.26	31.89
S3	64	10	10	15	1.0	2.0	5.29	32.44
S4	64	10	10	15	1.0	3.0	5.32	32.98
S5	64	10	10	15	1.0	5.0	5.40	33.92

2. Materials and methods

Five prototype oxide glasses were fabricated using 64TeO_2–10WO_3–10Nb_2O_5–15KF–1La_2O_{3-x}–Tm_2O_3 (where x=1, 2, 3, and 5 mol%) with density of 5.22–5.40 g/cm^3 and coded S1,

S2, S3, S4, and S5 (Table1). Calculations were made using Phy-X/PSD. This user-friendly online software is used to calculate parameters related to shielding and dosimetry with a wide range of ionizing radiation energy (26). The LAC is one of the parameters that can be calculated with this software. For a specific material thickness, LAC can evaluate the fraction of an attenuated incident with monoenergetic beams or photons, and thus it is able to estimate interactions of radiation with matter and assess Compton scattering, Rayleigh scattering, and photoelectric absorption or effect (27,28).Calculation of LAC is illustrated in the equation below, where I represents attenuated ionizing photons, I0 unattenuated ionizing photons, μ LAC (cm–1), and t the thickness (cm) of the simulated material:

$$I = I_0 e^{\mu - 1} \tag{1}$$

Another parameter that can be measured by this software is the MAC, also known as the mass absorption coefficient, which measures the ability of the ionizing photons to penetrate the material with determined density (28,29). the MAC can be expressed with the equation below, where MAC is represented by μm and material density by ρ.

$$\mu_{m=\frac{\mu}{\rho}} \tag{2}$$

The five prototype oxide glass that were fabricated contained more than one element, so to measure the MAC accurately, integrated weight of the fractional element wi was added to the equation:

$$\mu_m = \frac{\mu}{\rho} = \sum_i \; w_i \; (\mu/\rho)_i \tag{3}$$

Moreover, ACS and ECS were measured in Phy-X/PSD and used to determine the probability of incident ionization photons at selected energies, measured in cm2·g–1, where the Avogadro number is represented by NA, atomic weight Ai, atomic number Zi, and where the ith composition elements in the material of radiation shielding are the mol fraction fi:

$$\mathrm{ACS} = \sigma_T = \frac{\mu}{\rho} = \frac{\sum_i \; f_n A_n}{N_A} \; \mu \tag{4}$$

$$\mathrm{ECS} = \sigma_e = \left[\frac{1}{N_A}\right] \sum_i \; \left[\frac{f_i \, A_i}{Z_i} (\mu)_i\right] \tag{5}$$

One of the prime parameters is the material's HVL, which can be described as the thickness of material that decreases the intensity of radiation entering by half its original value and also the average travel distance of energetic photons between two successive collision-sequence interactions with radiation known as MFP. Both parameters can be derived using the LAC, and mathematically they can be expressed as follows (28,30).

$$\mathrm{HVL} = \frac{\ln 2}{\mu_L} \tag{6}$$

$$\mathrm{MFP} = \frac{1}{\mu_L} \tag{7}$$

As a result, high atomic number and electron density have a positive influence and contribute to increase effectiveness of the material that used in radiation protection. The effectiveness of the Zeff and Neff parameters are basic and considered in determining the penetration of radiation and photons in shielding materials (31). Both parameters are mathematically expressed as:

$$Z_{\mathrm{eff}} = \frac{\sigma_T}{\sigma_e} \tag{8}$$

$$N_{eff} = \frac{N_A}{\sum_i f_i A_i} Z_{eff} \sum \beta_{n_i} = \frac{\mu_m}{\sigma_e} \quad (9)$$

The parameter used for radiation-protection characteristics of the prototyped oxide glasses for shielding, defined as a multi-element material in terms of its elements, is the equivalent atomic number (Z_{eq}), and mathematically computed below, where (R_1 and R_2) represent the ratios of the MAC of Compton scattering to the MAC of the radiation shielding materials (μ_{comp}/μ_{total}), which has been calculated based on the atomic numbers(Z_1 and Z_2) for the selected elements (32)

$$Z_{eq} = \frac{Z_1 (\log R_2 - \log R) + Z_2 (\log R - \log R_1)}{(\log R_2 - Log R_1)} \quad (10)$$

Penetration of intonation radiation phonons into particular shielding materials provides two types of radiation photon: collided and uncollided. The EBF is the ratio of total specific radiation phonons when it reaches any point to the point of uncollided photons, and factor values can be obtained by using the geometric progress (GP) method (33). This method has been provided by American National Standard ANSI/ANS-6.4.3-1991(34). The parameters of GP fitting match the atomic number (Z_1 and Z_2), are appraised in the equation as C_1 and C_2, and the EBF equation can be expressed as such:

$$C = \frac{C_1 (\log Z_2 - \log Z_{eff}) + C_2 (\log Z_{eff} - \log Z_1)}{(\log Z_2 - Log Z_1)} \quad (11)$$

Further, EBF was measured using the equation below, and the distance between the radiation detector and ionizing radiation source are represented by x in MFP units. GP fitting parameters are expressed as K^x, b, a, and incident-photon energy as E and K (E, x), represent the dose multiplicative factor:

$$B(E, x) = 1 + \frac{(bC-1)}{(K-1)} (K^x - 1), K \neq 1 \quad (12)$$

$$B(E, x) = 1 + (b-1)x, K \neq 1 \quad (13)$$

$$B(E, x) = cx^a + d \frac{\tanh\left(\frac{x}{X_k} - 2\right) - \tanh(-2)}{1 - \tanh(-2)}, x \leq 40\, mfp \quad (14)$$

Finally, to calculate the capability of certain shielding materials to harden neutrons, the measurement must be used by fast neutron- removal cross section expressed in the below equation, where i and R the partial density. In this study, values of removal cross-section mass for the elements involved were taken from Chilton et al (1984) (35).

$$\Sigma_R = \sum_i \rho_n (\Sigma_R/\rho) i \quad (15)$$

Phy-X/PSD was utilized for all parameters calculation.

3. Results and discussion

Parameters of five prototyped radiation-shielding oxide glasses with different amounts of Tm_2O_3 (0–5 mol%) were calculated using Phy-X/PSD, and all simple were simulated ageist monoenergetic photon beams energy range between 15 keV to 15 MeV. LAC results are shown in Figure 1, and attenuation factors of the five samples gradually reduced as energy increased. Moreover, the addition of Tm_2O_3 in S_2–S_5 raised the density of oxide glass from 5.22 to 5.40 g/cm^3 and showed the highest LAC at 15 keV and 242.05–281.76 cm^2/g, while at 15 MeV the lowest attenuation values between (0.197–0.209 cm^2/g) were found. The S_1 sample without Tm_2O_3 showed the lowest density of other samples, the μ values at 80 keV and 8 MeV were 14.761 and

0.1777 cm^{-1}, respectively. At the same energy but high density in the S_5 sample, μ values were 17.031 and 0.1877 cm^{-1}, respectively. The difference between S_1 and S_5 at 80 keV was 14.28% and at 8 MeV 5.47%. Low photon transmission occurs at higher density, thus providing better oxide glass shielding due to the photons and atoms interacting to a greater in the attenuator (Noor Azman et al, 2013).

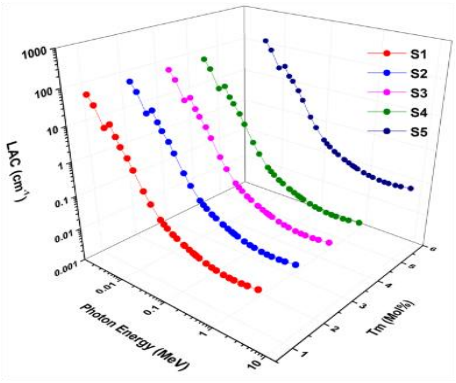

Fig. 1. 3D graph of the recorded results of LAC for all samples.

The MAC showed similar values, with differences between S_1 and S_5 at 80 keV of 10.90% and at 8 MeV 2.12% (Figure 2). Similarly, at the same density, the MAC for S_1 without doping at 6 keV and 4 MeV was 0.0346 and 4.59684 cm^2/g. However, the highest-density sample (S_5) showed a maximum mass absorption coefficient of 52.17 cm^2/g for all samples (Figure 2).

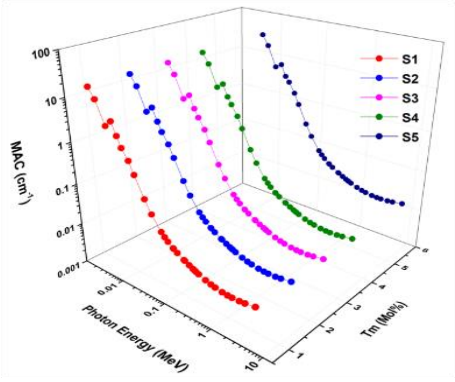

Fig. 2. 3D graph of the recorded results of MAC for all samples.

Additionally, at the same photon-beam energy range, all five oxide glasses had ACS and ECS measures. Glasses with higher absorption and attenuation of beam energy will have high ACS and ECS values, ie, material that with ACS and ECS is more effective for radiation-protection purposes. Adding Tm_2O_3 to the glass systems (Table 1) gradually increased their density and resulted in raised ACS and ECS values. For instance, the differences for S_5 at a density of 5.4 g/cm^3 at 15 keV and 15 MeV energy on ACS and ECS were 29.23% and 19.30%, respectively (Figures 3 and 4).

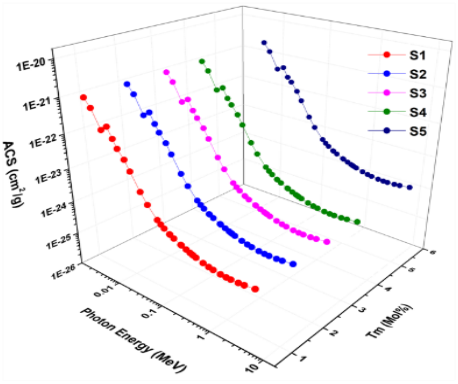

Fig. 3. 3D graph of the recorded results of ACS for all samples.

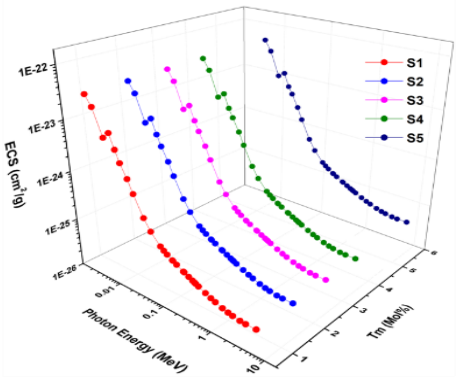

Fig. 4. 3D graph of the recorded results of ECS for all samples.

The HVL factor is important in assisting the materials utilized in radiation protection and to know the intensity or quality of beams through the materials. The HVL was computed for all samples (Figure 5). Initially, the minimum HVL of all samples was demonstrated, and then value escalated with rising energy. The addition of Tm_2O_3 increased the density and minimized the HVL, eg, S_1 and S_5 showed 5.22 and 5.40 g/cm^3, respectively, at 500 keV photon energy were recorded (6.1% difference).

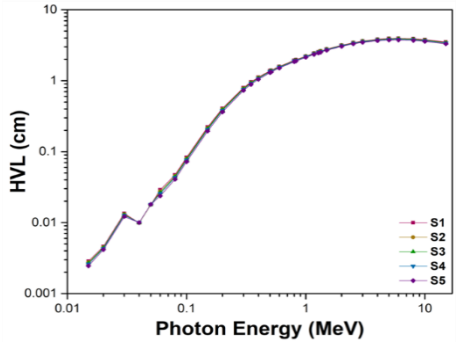

Fig. 5. Linear graph of the results of HVL for all samples.

While the best attenuation was in the S_5 system, which showed the HVL because of high weight doping of TeO_2, sample S_1 had the worst attenuation because it had the lowest density and was not doped with Tm_2O_3. As shown in Figure 5, HVL values rose as photon energy increased, indicating that the thickness of shielding must be increased for high photon energy. For instance,

HVL values for S_1–S_5 at 40 keV were 0.00989, 0.00991, 0.00995, 0.00999, and 0.01001 cm, and at 2 MeV escalated to 3.17002, 3.14271, 3.12186, 3.10138, and 3.05014 cm, respectively.

Various conventional concretes (barite, chromite, ferrite, and magnetite) and available commercial glasses (RS-520, RS-360 and RS-253) utilized for radiation shielding materials were compared for HVL values against the S_5 sample (36). As demonstrated in Figure 6, the HVL values of S_5 oxide glass and these concretes had the same energy.

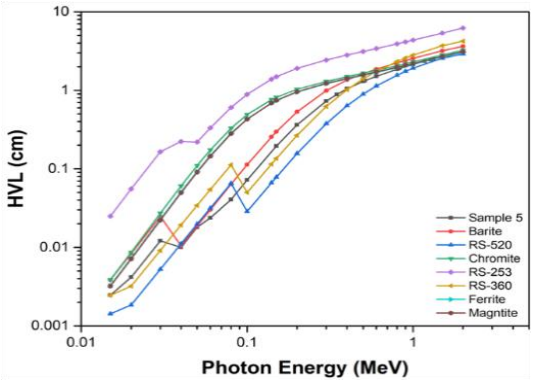

Fig. 6. Linear graph of the results of HVL for S_5 and comparisons with conventional concrete and commercial glasses.

The commercial shielding glass RS-253 HVL value was highest for the occurrence of γ photons compared to other concrete, commercial glasses, and S_5 oxide glass. At 2 MeV, ferrite and magnetite showed 3.059 and 3.1 cm, while the S_5 sample at similar energy showed 3.05 cm and RS-520 commercial glass at similar energy 2.9 cm, the lowest HVL. Based on the outcome, the S_5 glass could be effectively utilized for radiation-protection applications, especially where low beam energy is applied, such as in radiology.

Another essential factor is the MFP, and it was evaluated in this study. The MFP is used to evaluate radiation-protection material, and it can explain the interaction between occurrence of radiation photons and shielding-material atoms. Shown in Figures 7 and 8 are the computed MPF values of the five glasses, conventional concrete, and commercial glass shielding materials. MPF values showed trends similar to HVL: high-density materials achieved low MPF values. Also, increasing the density of the glass samples by adding Tm_2O_3 enhanced MFP values.

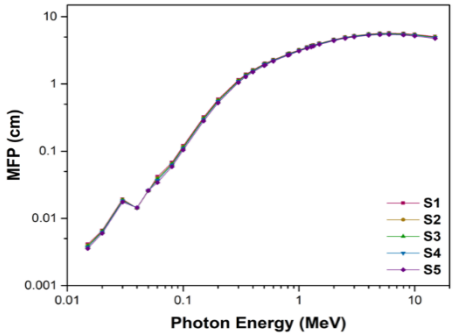

Fig. 7. Linear graph of the results of MFP for all samples.

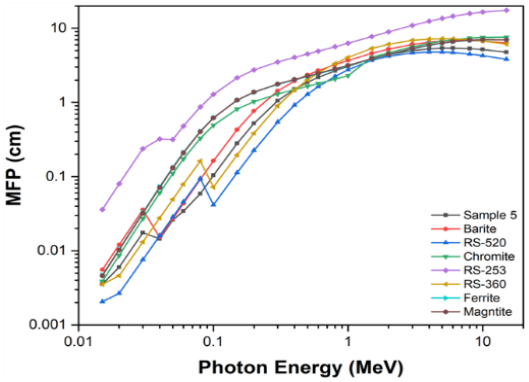

Fig. 8. Linear graph of the results of MPF for S5 and comparison with conventional concrete and commercial glasses.

Two more essential parameters are Z_{eff} and N_{eff}. These were utilized to identify and understand the shielding materials' interaction with incident ionizing radiation (Figures 9 and 10). The addition of Tm_2O_3 to glass samples were examined for Z_{eff} and N_{eff} trends at various energies. The highest Tm_2O_3 fraction was in sample S5, which also obtained the highest Z_{eff} and N_{eff} values. Increased Tm_2O_3 in the glass systems was more burdened by interaction with photon energy. MAC and ECS are strongly correlated with N_{eff} values and protuberance in the curves can be seen in Figure 10 for all oxide glasses, which explains the K-shell absorption edges.

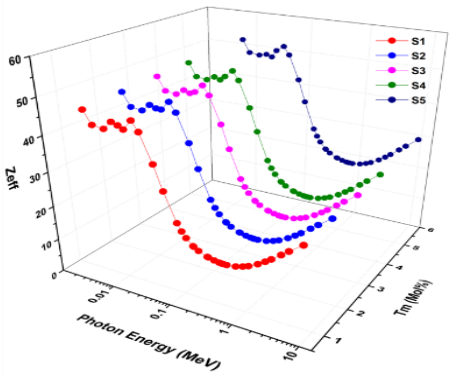

Fig. 9. 3D graph of the recorded results of Z_{eff} for all samples.

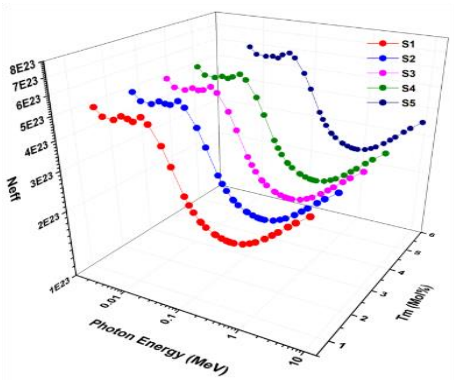

Fig. 10 . 3D graph of the recorded results of N_{eff} for all samples.

The EBF assessed a variety of photo energies range between 15 keV and 15 MeV. As illustrated in Figure 11, EBF values for all samples were high at higher energies and low at lower energies, indicating pair-production and photoelectric effects. At the lowest energies of photoelectric absorption, most photon absorption occurs devoid of second interactions of propagation or formation.

Because of the Compton effect, the interactions of photons were not fully absorbed by the samples between 40 KeV and 0.06MeV and showed high EBF values. On the other hand, slight interactions and higher penetration of samples occurred at high energy and resulted in high EBF values, escalating the depth of penetration. As demonstrated in Figure 11, the effect of the addition of Tm_2O_3 and was high EBF values at lower energies.

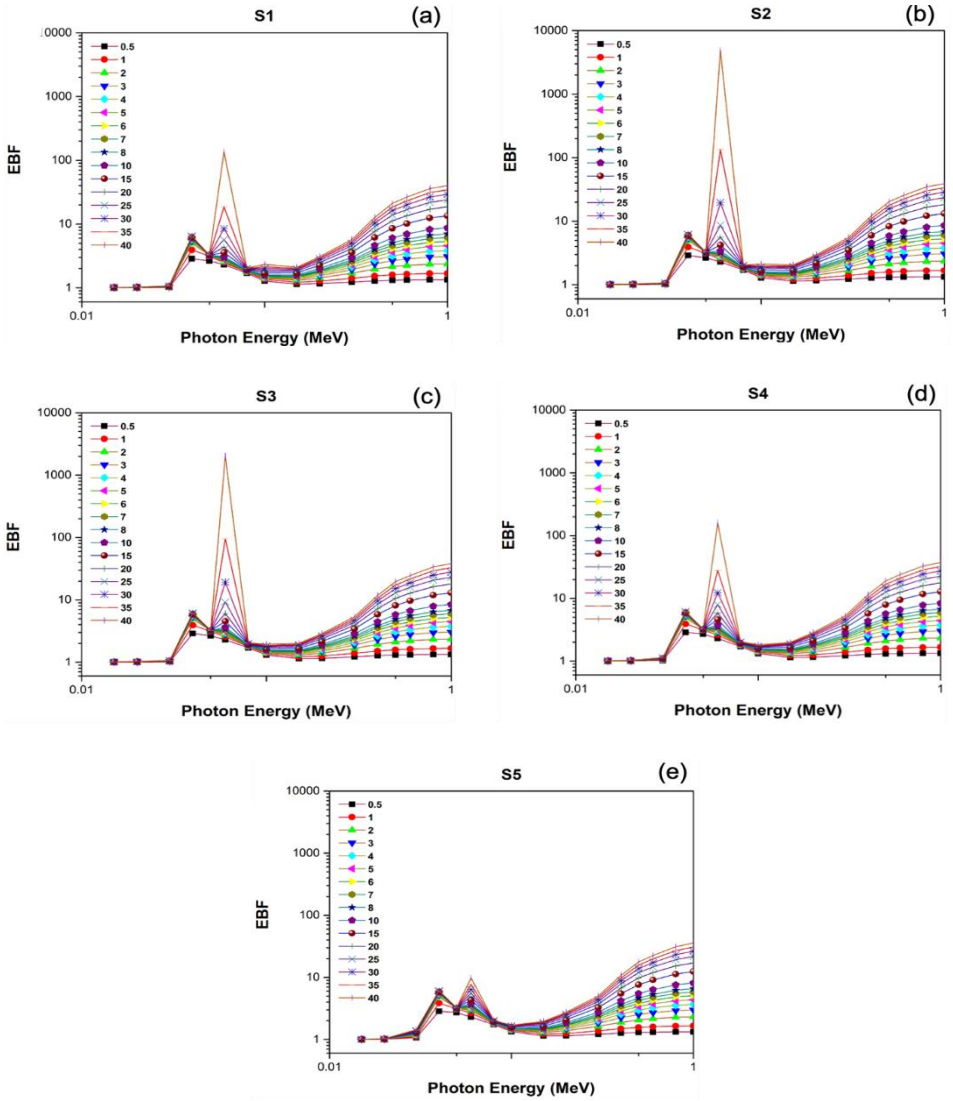

Fig. 11. Linear graph of the results of EBF for all samples: Sample 1(a), Sample 2(b), Sample 3(c), Sample 4(d) and Sample 5(e).

4. Conclusion

Phy-X/SPD was used to evaluate various parameters to understand high and low photon-energy effects on the five samples. The highest LAC values were between 242 and 281 cm^2/g at 15 keV. S_5 was the densest, showing maximum MAC of 52.17 cm^2/g. ACS and ECS values were effectively increased with the addition of Tm_2O_3 to the glass systems. HVL values were compared

against conventional concretes and available commercial glass types. RS-253 glass was higher for the occurrence of γ photons compared to all materials, while S_5 and RS-520 at 2 MeV showed 3.05 and 2.9 cm. MPF showed behavior similar to HVL: high-density materials achieved low MPF values. Also, increasing the density of our glasses by adding Tm_2O_3 enhanced MFP values. The highest Z_{eff} and N_{eff} values were recorded on S_5 glass, because it had the highest Tm_2O_3 fraction and was more burdened by interaction with photon energy. EBF values for all samples were high at higher energies and low at lower energies.

Acknowledgments

The authors extend their appreciation to the Deanship of Scientific Research at King Khalid University (KKU) for funding this research project Number (R.G. P2/79/41).

References

[1] N. Simon, American journal of public health and the nation's health, **57** (1964).
[2] D. A. Gollnick, Basic radiation protection technology 3rd edition, United States: Pacific Radiation Corporation; 1994. Available from: http://inis.iaea.org/search/search.aspx?orig_q=RN:26063146
[3] M. Donya, M. Radford, A. ElGuindy, D. Firmin, M. H. Yacoub, Global cardiology science & practice **4**, 437 (2014).
[4] K. Kamiya, M. Sasatani, Nihon rinsho Japanese journal of clinical medicine **70**(3), 367 (2012).
[5] S. Balter, J. W. Hopewell, D. L. Miller, L. K. Wagner, M. J. Zelefsky, Radiology **254**(2), 326 (2010).
[6] C. Betlazar, R. J. Middleton, R. B. Banati, G.-J. Liu, Redox biology **9**, 144 (2016).
[7] H. Issard, In: Sorenson KBBT-S and ST and S of RM, editor. Oxford: Woodhead Publishing, 123 (2015).
[8] R. W. Roussin, B. L. Kirk, In: Meyers RABT-E of PS and T (Third E, editor. New York: Academic Press, 581 (2003).
[9] C. Allen, L. Manson, In: Devgun JBT-MNP, editor. Woodhead Publishing Series in Energy. Woodhead Publishing, 136 (2013).
[10] D. Adlienė, L. Gilys, E. Griškonis, Nuclear Instruments and Methods in Physics Research Section B: Beam Interactions with Materials and Atoms **467**, 21 (2020).
[11] N. Healey, Radiation Protection Dosimetry **134**(3–4), 143 (2009).
[12] S. A. M. Issa, M. I. Sayyed, A. M. A. Mostafa, G. Lakshminarayana, I. Kityk, Journal of Materials Science: Materials in Electronics **30**(13), 12140 (2019).
[13] M. S. Al-Buriahi, V. P. Singh, A. Alalawi, C. Sriwunkum, B. T. Tonguc, Ceramics International **46**(10, Part A), 15464 (2020).
[14] T. Kosuge, Y. Benino, V. Dimitrov, R. Sato, T. Komatsu, Journal of Non-Crystalline Solids **242**(2), 154 (1998).
[15] H. A. OTHMAN, M. M. ALQAHTANI, M. REBEN, EL S. YOUSEF, RAMAN GAIN AND STRUCTURAL OF TELLURITE-PHOSPHATE GLASSES WITH DIFFERENT MODIFIERS DOPING WITH Er2O3, Chalcogenide Letters **17**, (4), 207 (2020).
[16] G. Susoy, Ceramics International **46**(3), 3844 (2020).
[17] F. Laariedh, O. Alatawi, M. S. Al-Buriahi, M. I. Sayyed, T. B. Badeche, Applied Physics A **126**(1), 30 (2019).
[18] E. F. el Agammy, H. Doweidar, K. El-Egili, R. Ramadan, M. Jaremko, A.-H. Emwas, Ceramics International **46**(11, Part B), 18551 (2020).
[19] K. Linganna, J.-H. In, S. H. Kim, K. Han, J. H. Choi, Materials **13**, 2020.
[20] N. Elkhoshkhany, S. Y. Marzouk, S. Shahin, Journal of Non-Crystalline Solids **472**, 39 (2017).

[21] N. S. Tagiara, D. Palles, E. D. Simandiras, V. Psycharis, A. Kyritsis, E. I. Kamitsos, Journal of Non-Crystalline Solids **457**, 116 (2017).
[22] A. Palui, A. Ghosh, AJournal of Non-Crystalline Solids **482**, 230 (2018).
[23] N. ELKHOSHKHANY, MAI MAHMOUD, EL SAYED YOUSEF, STRUCTURAL, THERMAL AND OPTICAL PROPERTIES OF NOVEL OXYFLUOROTELLURIDE GLASSES, Chalcogenide Letters **16**, (6), 265 (2019).
[24] A. S. Altowyan, M. I. Sayyed, Y. Al-Hadeethi, Applied Physics **A126**(6), 464 (2020).
[25] M. K. Halimah, A. Azuraida, M. Ishak, L. Hasnimulyati, Journal of Non-Crystalline Solids **512**, 140 (2019).
[26] E. Şakar, O. F. Özpolat, B. Alım, M. I. Sayyed, M. Kurudirek, Radiation Physics and Chemistry **166**, 108496 (2020).
[27] W. Huda, R. M. Slone, RM. Review of Radiologic Physics [Internet]. Lippincott Williams \& Wilkins; 2003. (High-Yield Systems Series).
[28] D. S. Chang, F. D. Lasley, I. J. Das, M. S. Mendonca, J. R. Dynlacht, In: Chang DS, Lasley FD, Das IJ, Mendonca MS, Dynlacht JR, editors. Cham: Springer International Publishing, 69 (2014).
[29] Jacob Beutel, H. L. Kundel, R. L. van Metter, Handbook of medical imaging **1**, Bellingham, Wash.: SPIE; 2000.
[30] Erik A. Aydogmuş, E. Kavaz, S. Ilkbahar, U. Kara, C. E. Erik, H. O. Tekin, Results in Physics **13**, 102354 (2019).
[31] S. Gowda, S. The Mass Attenuation Coefficients, Effective Atomic Cross Sections, Effective Atomic Numbers and Electron Densities of Some Halides. 2016 Jul 5 [cited 2021 Apr 5].
[32] M. I. Sayyed, F. Q. Mohammed, K. A. Mahmoud, E. Lacomme, K. M. Kaky, M. U. Khandaker et al., Applied Sciences **10**, 2020.
[33] M. I. Sayyed, M. Y. AlZaatreh, K. A. Matori, H. A. A. Sidek, M. H. M. Zaid, Results in Physics 9, 585 (2018).
[34] D. Trubey, C. Eisenhauer, A. Foderaro, D. Gopinath, Y. Harima, J. Hubbell et al., American National Standard ANSI/ANS-; 1991.
[35] A. B. Chilton, R. E. Faw, Kenneth Shultis, Principles of radiation shielding. Englewood Cliffs: Prentice-Hall; 1984.
[36] M. S. Alqahtani, A. M. Almarhaby, K. I. Hussein, Y. M. AbouDeif, H. Afifi, H. Zahran et al., Journal of Instrumentation **16**(01), P01002 (2021).